Intermetallic ordering and structure in Fe–Pd alloy nanoparticles

Kazuhisa Sato,[1,2,3,a)] J. G. Wen,[2] and J. M. Zuo[1,2,b)]
[1]*Department of Materials Science and Engineering, University of Illinois at Urbana-Champaign, Urbana, Illinois 61801, USA*
[2]*Frederick Seitz Materials Research Laboratory, University of Illinois at Urbana-Champaign, Urbana, Illinois 61801, USA*
[3]*The Institute of Scientific and Industrial Research, Osaka University, Ibaraki, Osaka 567-0047, Japan*

(Received 1 November 2008; accepted 29 March 2009; published online 5 May 2009)

We report an *in situ* study of epitaxial island formation and alloying of FePd nanoparticles using reflection high-energy electron diffraction (RHEED) followed by *ex situ* atomic structure characterization. We used aberration corrected (AC) scanning transmission electron microscopy (STEM) with a high-angle annular dark field (HAADF) detector for the study of chemical ordering. The FePd nanoparticles were formed by sequential deposition of Pd and Fe onto NaCl substrates, which was then followed by heating to high temperatures to promote chemical ordering during a short period of annealing. We show that the epitaxial island growth and subsequent alloying of Fe into Pd can be clearly detected by RHEED. The high resolution and the atomic number (Z) contrast of AC HAADF-STEM allow a clear observation of nanometer-sized local chemical order in very small nanoparticles. The results revealed complex chemical structures at an intermediate stage of the ordering process with ordered regions of both $L1_0$ and $L1_2$ phases. © *2009 American Institute of Physics*. [DOI: 10.1063/1.3122601]

I. INTRODUCTION

The FePd alloy nanoparticles with the $L1_0$-type ordered structure is one of the candidate materials suitable for future ultrahigh-density magnetic storage media. The $L1_0$ FePd alloy has a high magnetocrystalline anisotropy energy (MAE) and high saturation magnetization.[1] The reported value for the MAE constant (K_u) is as high as 1.7×10^6 J/m^3 (Ref. 2). The high MAE originates from the tetragonal ordered structure with alternate stacking of Fe and Pd in [001] direction (c-axis) and it has been reported that the MAE is proportional to the square of the degree of order.[3] Nanoparticles of sufficiently small sizes can be formed with a single domain and their magnetization process is carried out by rotation magnetization. The latest report shows that FePd nanoparticles as small as 10 nm have a very large room temperature coercivity, which is suitable for ultrahigh-density magnetic storage media.[4]

Alloy nanoparticles of FePd, or other similar compounds such as FePt, can be synthesized by chemical solution methods[5–7] or physical vapor deposition.[8–10] As-prepared nanoparticles are either disordered solid solutions or nanocomposites of Fe and Pt (Pd) characterized by low magnetocrystalline anisotropy energies. High temperature annealing is required to form the ordered $L1_0$ phase. However, previous studies have shown that it is difficult to achieve a high degree of long-range order (LRO) in small nanoparticles by annealing.[11] Nanobeam electron diffraction analysis of the LRO parameter of $L1_0$-FePd nanoparticles by one of the authors showed a size-dependent decay.[12] A reduction in the coercivity of the FePd nanoparticles was observed in conjunction with the decay of LRO.[4]

Here we report on the chemical ordering process and the nature of reduced LRO in FePd nanoparticles using a combination of *in situ* reflection high-energy electron diffraction (RHEED) observations and *ex situ* high resolution imaging by aberration-corrected high angle annular dark-field (HAADF) scanning transmission electron microscopy (STEM). The FePd nanoparticles studied were formed as epitaxial islands on a NaCl substrate using sequential deposition of Pd followed by Fe based on a previously reported procedure.[10,12] The formation of epitaxial islands and the alloying process of Fe–Pd nanoparticles were followed by RHEED during deposition and the postdeposition annealing. The improved resolution and chemical sensitivity of aberration-corrected HAADF-STEM compared to conventional high resolution electron microscopy (HREM)[10–12] are used to detect chemical ordering in the small nanoparticles. We show that the combination of *in situ* RHEED and aberration-corrected HAADF-STEM provides quantitative information about the ordering process, formation temperature, and the nature of ordering in alloyed nanoparticles.

II. EXPERIMENTS

FePd nanoparticles were prepared by successive deposition of high-purity Pd (99.99%) and Fe (99.995%) onto single-crystal NaCl(001) substrates at 560–570 K using electron-beam (EB) deposition. The substrate crystals were cleaved in air and supplied to a high vacuum EB chamber (base pressure of $\sim10^{-7}$ Pa). The amount of Fe and Pd deposited is measured in term of the film thickness monitored by using a quartz oscillator. The film thickness is expressed

a)Present address: Institute for Materials Research, Tohoku University, Katahira, Aoba-ku, Sendai 980-8577, Japan.
b)Electronic mail: jianzuo@uiuc.edu.

TABLE I. Deposited thickness, substrate temperatures, and annealing conditions for the FePd nanoparticles grown on NaCl(001) single crystal substrates.

Sample No.	Thickness	Substrate Temp.	Postdeposition Annealing
1	Fe(7.0 ML)/Pd(6.7 ML)	570 K	835 K-10 min
2	Fe(5.6 ML)/Pd(6.2 ML)	560 K	785 K-5 min
3	Fe(7.0 ML)/Pd(6.7 ML)	570 K	865 K-10 min
4	Fe(7.0 ML)/Pd(6.7 ML)	570 K	775 K-10 min

in the unit of monolayer (ML), which corresponds to the (200) plane spacing of Fe or Pd (0.143 nm for Fe, and 0.195 nm for Pd). For *ex situ* TEM and STEM observations, we deposited a thin film of Al_2O_3 (99.99%) as support, which also helps to protect parts of the FePd nanoparticles against oxidation. The deposition and subsequent annealing were carried out in the EB chamber equipped with a RHEED gun. The growth rate was monitored using a quartz oscillator and calibrated by *ex situ* Rutherford backscattering spectroscopy. The growth rate was set at 0.1 nm/min for Pd and Fe, and at 0.5 nm/min for Al_2O_3. The surface of the NaCl(001) substrate prior to the epitaxial growth and alloying of nanoparticles was characterized by RHEED. The RHEED patterns were recorded using a charge coupled device (CCD) camera. A tungsten-rhenium thermocouple attached to the sample heater was used to monitor the sample temperatures. The temperature at the sample position was calibrated using a chromel-alumel thermocouple. After deposition at the substrate temperatures of 560–570 K, the specimens were heated continuously up to the temperatures of 775–865 K and held at these final temperatures for 5–10 min. The samples were then gradually cooled down to room temperature. The heating and the cooling rate were set to approximately 3 and 6 K/min, respectively. The detailed conditions for the preparation of each sample studied here, including the as-deposited thickness, the substrate temperature during deposition, and the maximum annealing temperature, are listed in Table I. Particle morphology, HREM images, and selected area electron diffraction (SAED) patterns were observed *ex situ* by using a JEOL 2010F TEM (C_s=1.0 mm) operating at 200 kV with a field emission gun (FEG). The HAADF-STEM images were recorded *ex situ* using the JEOL 2200FS [equipped with a FEG and a Corrected Electron Optical Systems, GmbH (CEOS), probe corrector] installed at the Materials Research Laboratory, University of Illinois. The microscope was operated at 200 kV. The alignment of the microscope and the aberration corrector was done following the standard equipment procedure. The corrector was further adjusted based on the Ronchigrams obtained from the amorphous Al_2O_3 region for defocus and astigmatism. Details of the performance of this microscope have been reported in literature.[13] For *ex situ* TEM and STEM observations, the NaCl(001) substrate was dissolved in distilled water and the free-standing sample films were picked up and mounted on the Cu grids. All TEM and STEM images were recorded by using CCD cameras attached to the microscopes.

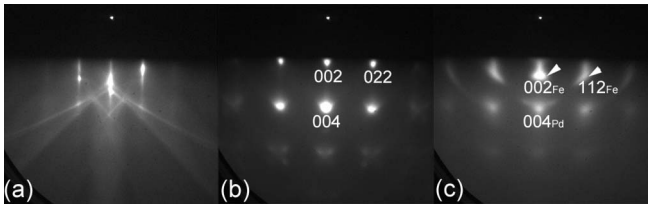

FIG. 1. RHEED patterns recorded *in situ* during the epitaxial growth of nanoparticles supported on NaCl(001) at 570 K (sample #1). The beam incidence is parallel to $[100]_{NaCl}$ with glancing angle of 2.7°. (a) NaCl(001) before Pd deposition, (b) after deposition of Pd with 6.7 ML coverage, and (c) after deposition of Fe with 7.0 ML coverage. Epitaxial island formation is clearly seen by spotlike fcc-Pd and bcc-Fe reflections. The orientation relationship between Pd and NaCl and Fe and Pd are as follows: $[100]_{Pd}\|[100]_{NaCl}$, $(001)_{Pd}\|(001)_{NaCl}$, and $[\bar{1}10]_{bcc\text{-}Fe}\|[100]_{Pd}$, $(001)_{bcc\text{-}Fe}\|(001)_{Pd}$.

III. RESULTS AND DISCUSSION

A. Epitaxial island formation and alloying observed by RHEED

Figure 1 shows a series of RHEED patterns recorded during the course of deposition for a total coverage of 6.7 and 7.0 ML of Pd and Fe, respectively (sample #1). Before the Pd deposition, the NaCl(001) gave clear sharp diffraction streaks in the recorded RHEED pattern indicating a smooth substrate surface [Fig. 1(a)]. The diffraction patterns were recorded using the beam incidence along $[100]_{NaCl}$ at 13 kV (λ=0.0107 nm). The electron incident angle was 2.7°. After depositing a small amount of Pd at 570 K, diffraction streaks from the NaCl surface disappeared and a clear diffraction pattern with spotlike Pd reflections was obtained. The diffraction pattern belongs to the [100] zone axis of the Pd with a face centered cubic (fcc) structure. The epitaxial orientation relationship observed is $[100]_{Pd}\|[100]_{NaCl}$, $(001)_{Pd}\|(001)_{NaCl}$. This cube-cube orientation relationship is in agreement with previous reports[14–16] in spite of a large lattice mismatch of 31% compared to a mismatch of −2.5% for the epitaxial relationship of Pd[110]‖NaCl[100] (Ref. 17). The preference of a large misfit in one orientation relationship over a smaller misfit in another orientation relationship has been observed before, for example, in the case of Ag(100)‖Si(100) with Ag[011]‖Si[011] and a mismatch of −25% (Ref. 18). LeGoues *et al.*[19] pointed out that the real misfit between two lattices is not always the determining factor for epitaxy. For Ag(111)‖Si(111), LeGoues *et al.*[19] constructed a 4(Ag):3(Si) coincident-site lattice to explain the $Ag[\bar{1}10]\|Si[\bar{1}10]$ epitaxial relationship. In this case, the observed cube-cube orientation epitaxy can be explained based on a coincidence cell of 3 (Pd): 2 (NaCl), which gives a mismatch of 3.4%.

The spotlike Pd reflections in Fig. 1 are due to the island growth of Pd and the glancing angle diffraction geometry, which gives a transmission like diffraction pattern. The Fe was deposited onto the already formed Pd islands and the NaCl substrate. The deposited Fe also gave spotlike reflections in the recorded diffraction patterns. The diffraction pattern can be indexed based on the body centered cubic (bcc) structure. The beam incidence is along the $[\bar{1}10]_{Fe}$. In Fig. 1(c), clear $(002)_{Fe}$ and $(112)_{Fe}$ (as indicated by the arrow-

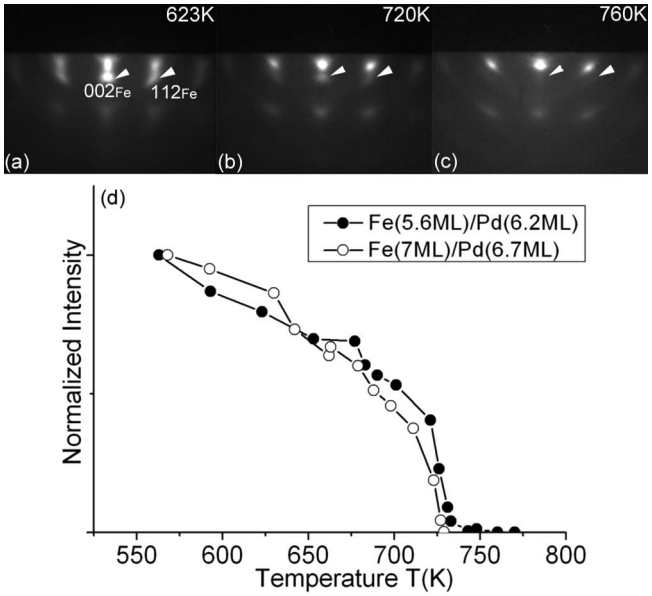

FIG. 2. RHEED patterns recorded *in situ* from epitaxial Fe/Pd nanoparticles supported on NaCl(001) during the postdeposition annealing (sample #2). The Fe and Pd coverage are 5.6 and 6.2 ML, respectively. The beam incidence is parallel to $[100]_{NaCl}$ with glancing angle of 1.6°. (a) 623 K, (b) 720 K, and (c) 760 K. Reflections from bcc-Fe indicated by arrowheads gradually disappeared on annealing due to alloying of Fe into Pd. Change in $(112)_{Fe}$ reflection intensity during the *in situ* annealing is shown in (d). For comparison, intensity change of Fe(7.0 ML)/Pd(6.7 ML) nanoparticles (sample #3) is also plotted. Intensity of $(112)_{Fe}$ reflection rapidly dropped at temperatures between 710 and 730 K, for both specimens.

heads) reflections are seen in addition to the diffraction spots of Pd with the fcc structure. The orientation relationship between the bcc Fe and the fcc Pd is as follows: $[\bar{1}10]_{BCC\text{-}Fe} \| [100]_{Pd}$, $(001)_{BCC\text{-}Fe} \| (001)_{Pd}$. According to this orientation relationship, lattice mismatch between Fe and Pd is calculated to be $(\sqrt{2}a_{Fe}-a_{Pd})/a_{Pd}\times 100=4.2\%$, where $a_{Fe}=0.286\ 64$ nm and $a_{Pd}=0.389\ 07$ nm are the lattice parameters of Fe and Pd, respectively.[20] Note that this orientation relationship between Fe and Pd arises from the epitaxial growth of Fe onto Pd nanoparticles.[9,10] Also note that there is no evidence of alloying or ordering of Fe and Pd in the RHEED patterns for as-deposited samples. After the deposition of Al_2O_3, the RHEED pattern showed only a halo pattern from the amorphous Al_2O_3 film.

To monitor the alloying of Fe and Pd during postdeposition annealing, some of the specimens were annealed *in situ* without the Al_2O_3 coating. The RHEED patterns shown in Fig. 2 are snapshots (exposure time less than a second) recorded during the heating process at (a) 623 K, (b) 720 K, and (c) 760 K. The maximum annealing temperature was 785 K. The amounts of Fe and Pd deposited are equivalent to 5.6 and 6.2 ML coverage, respectively (sample #2). The diffraction patterns were recorded using the electron beam incidence along $[100]_{Pd}$ at 12 kV ($\lambda=0.0111$ nm). The incident angle of the electrons was 1.6°. Diffraction spots belonging to $(002)_{Fe}$ and $(112)_{Fe}$, as indicated by the arrowheads, gradually become weak in intensity as the annealing temperature increases. The Fe diffraction spots finally disappear at 760 K [Fig. 2(c)] and leave behind only those diffraction spots belonging to the fcc structure. The disappearance of the bcc Fe reflections indicates the alloying of Fe into Pd nanoparticles [some weak diffraction rings can be seen in Fig. 2(c) indicating that the alloying is not complete]. To monitor the alloying of Fe, the intensity of the $(112)_{Fe}$ reflection was measured as a function of the annealing temperature. The measured intensity was normalized by the background intensity of the RHEED pattern. Figure 2(d) shows the temperature dependence of the $(112)_{Fe}$ intensity (used to monitor the alloying) for samples with a coverage of Fe(5.6 ML)/Pd(6.2 ML) (sample #2) and Fe(7.0 ML)/Pd(6.7 ML) (sample #3). The measured Fe intensity gradually decreases as the temperature increases, and rapidly drops in the narrow temperature range between 710 and 730 K for both samples. When the bcc Fe reflections disappeared, the lattice spacing of $(200)_{Pd}$ decreased by 2%, which is another indication of the alloying of Fe into Pd. *Ex situ* TEM observation showed that postdeposition annealing at 763 K lead to a partial formation of the $L1_0$-type ordered phase in FePd nanoparticles, which was confirmed by the appearance of weak superlattice reflections on SAED patterns and also by lattice images of the tetragonal ordered structure. According to the previous study based on *in situ* TEM annealing,[21] the initial appearance of weak superlattice reflections was detected at 723 K, and its intensity increased as the temperature rose. However, in this study, the superlattice reflections from the ordered phase could not be detected by RHEED at temperatures up to 785 K. The structure factors of the superlattice reflections of the equiatomic $L1_0$ structure are much smaller than those of the fundamental reflections. It appears that RHEED patterns recorded here are not sensitive to very weak reflections. Dynamical scattering effect may change the intensity ratios of strong and weak reflections somewhat but it is not expected to affect the overall picture here.[12] The other possibility is that the surface of the nanoparticles is less ordered than the interior. Because electrons at the glancing angle in the RHEED geometry are more sensitive to layers near the surface, difference in ordering between the surface and the interior also affects the diffraction pattern. Nonetheless, alloying between Fe and Pd clearly can be monitored based on the intensities of the fundamental reflections as we showed here.

B. Structure and atomic ordering observed by HREM and SAED

The structure and morphology of FePd alloy nanoparticles were characterized by TEM. A TEM image, SAED pattern, and HREM image of FePd alloy nanoparticle are shown in Figs. 3(a)–3(c), respectively. The SAED pattern was recorded over an area with many nanoparticles as shown in Fig. 3(a). The sample was prepared with Fe and Pd coverages of 7.0 and 6.7 ML, respectively (sample #4). The sample was annealed at 775 K for 10 min after deposition. The TEM observations show that epitaxial FePd nanoparticles with sizes of about 10 nm were formed and dispersed on the substrate surface [Fig. 3(a)]. Weak (110) superlattice reflections of the $L1_0$ ordered structure are seen on the corresponding SAED pattern in Fig. 3(b). The weak diffraction spots, as indicated by the double arrowhead, are indexed as the $\{110\}_{Fe}$ reflections of bcc Fe, which belongs to a minor

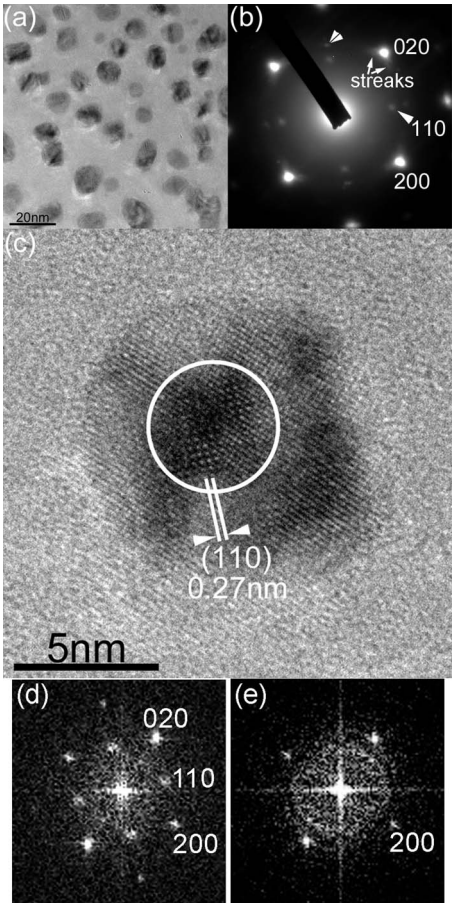

FIG. 3. TEM results for FePd nanoparticles after annealing at 775 K for 10 min. Coverage of Fe and Pd are 7.0 and 6.7 ML, respectively (sample #4). The average composition is Fe-58at. % Pd. (a) BF TEM image, (b) corresponding SAED pattern, and (c) HREM image. Weak $(110)_{FePd}$ superlattice reflection is seen on the SAED pattern. Lattice fringes of (110) from the $L1_0$ ordered structure is seen only at the center of the nanoparticle, indicating the initial stage of atomic ordering with low degree of chemical order. In this encircled area, crystallographic *c*-axis of the tetragonal ordered structure oriented normal to the substrate surface. (d) FT pattern of the ordered region. (e) FT pattern of the disordered peripheral region.

orientation relationship not seen in the RHEED patterns. These Fe reflections are rotated by 45° around the axis normal to the film compared to the dominant epitaxial orientation relationship between Fe and Pd [see Figs. 1(c), 2(a), and 2(b)]. In Fig. 3(b), the weak diffraction streaks seen around the {200} fundamental reflections are possibly caused by defects ({111} twins and stacking faults) in nanoparticles according to a previous report.[22] The (001) and (110) superlattice reflections correspond to ordered regions with their *c*-axes oriented parallel and normal to the substrate surface, respectively. The absence of the (001) superlattice reflection in the diffraction pattern, thus, indicates the preferential growth with the *c*-axis along the surface normal direction. An example of local ordering with the *c*-axis normal to the substrate surface (hereafter, *c*-domain) observed by HREM is shown in Fig. 3(c). A Fourier transform (FT) of the encircled area of the particle in Fig. 3(c) is shown in Fig. 3(d). This pattern is consistent with the formation of the *c*-domain of the $L1_0$ ordered structure. The ordered region has a size of ~4 nm in diameter, while the nanoparticle is 10 nm in size. The ordered region is characterized by the {110} lattice spacing of 0.27 nm of the ordered structure. This was not observed outside of the small ordered region. The lattice fringes seen outside of the ordered region are indexed as the {200} of the fcc lattice. A FT pattern obtained from the disordered peripheral region is shown in Fig. 3(e). The average alloy composition of this specimen was Fe-58at. % Pd based on the elemental analyses using energy dispersive x-ray spectrometer (EDX) attached to the TEM.

To check the effects of atomic diffusion on the evolution of chemical order, we also performed annealing at a higher temperature, at 835 K for 10 min (sample #1, average composition: Fe-58at. % Pd). In this case, we see pieces of evidence that the chemically ordered region somewhat increased at the center of nanoparticles. However, the intensities of the (110) reflections were still weak, indicating a low degree of order.

Besides the (110) superlattice reflections, we also observed faint (001) superlattice reflections in the recorded SAED patterns. The intensities of the (001) superlattice reflections, however, are much weaker compared to those of the (110) reflections. The weak (001) is consistent with FePd nanoparticles with the *c*-axis either normal or parallel to the substrate; the majority of particles have the *c*-axis normal to the substrate in agreement with previous studies.[10,23]

C. Atomic resolution imaging of chemical order observed by C_s-corrected HAADF-STEM

To clarify the atomic structure of the annealed FePd nanoparticles, we carried out aberration-corrected HAADF-STEM imaging. Figure 4 shows several HAADF-STEM images for the FePd nanoparticles (sample #1, average composition: Fe-58at. % Pd) after annealing at 835 K for 10 min. The short annealing time was designed to observe possible intermediate structures of the alloyed nanoparticles. The sizes of nanoparticles in Fig. 4 are 4 nm (a), 6 nm (b), 8 nm (c), 9 nm (d), and 11 nm (e). In each case, different types of image contrast seen in the nanoparticle are highlighted on the right. In Fig. 4(a), an atomic image of $L1_2$ ordered structure is seen at the center of the nanoparticle. The crystal structure is judged from the FT pattern with characteristic {100} and {110} superlattice reflections and the distinctive image contrast (top right) compared to peripheral areas (bottom right). The (100) lattice is present in the $L1_2$ phase but not in the $L1_0$. The number of (100) lattice fringes is only seven, indicating the formation of a very small ordered region about 2 nm in size. Another example of partial formation of the $L1_2$ phase is shown in Fig. 4(b). The $L1_2$ ordered structure is also observed at the central part of the nanoparticle shown in Fig. 4(e), while the periphery in this case shows the $L1_0$ structure. Partially ordered regions with (110) and (001) fringes of the $L1_0$ structure are seen in the 8 nm-sized FePd nanoparticle [Fig. 4(c)]. The FT pattern shown in the inset of Fig. 4(c) (upper left) shows the +/−(001) reflections in addition to the four {110} spots. This clearly indicates the existence of two ordered variants with a difference in the *c*-axis orientation, one normal and the other parallel to the substrate. The evidence of nanoparticles with multiple ordering variants after a short time annealing (5–10 min) suggests that the initial or-

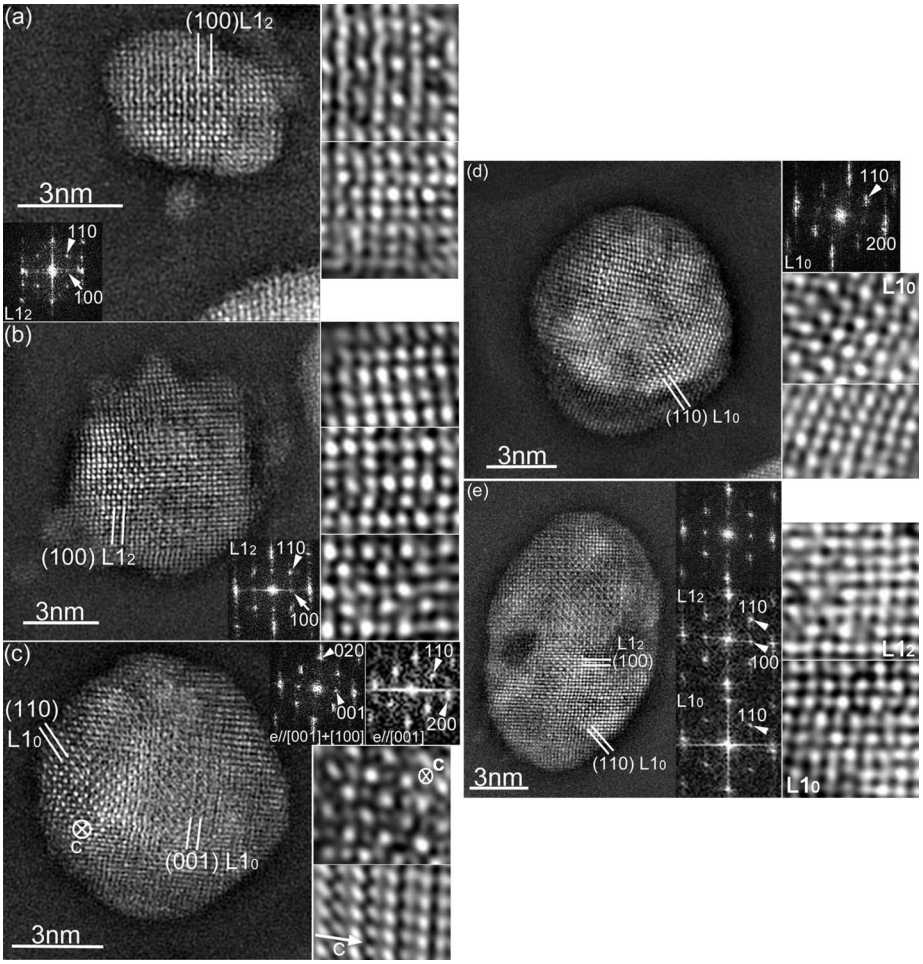

FIG. 4. *Z*-contrast images by C_s-corrected HAADF-STEM for FePd nanoparticles after annealing at 835 K for 10 min (sample #1). The average composition is Fe-58at. % Pd. Nanoparticle sizes and the beam incidences are as follows: (a) 4 nm, [001]$L1_2$, (b) 6 nm, [001]$L1_2$, (c) 8 nm, [001]$L1_0$ +[100]$L1_0$, (d) 9 nm, [001]$L1_0$, and (e) 11 nm, [001]$L1_0$+[001]$L1_2$. Corresponding Fourier spectra show the difference between the $L1_0$- or $L1_2$-type ordered structures. The high magnification images on the right are selected from areas of the nanoparticles with different image contrast. Chemically ordered region is clearly imaged as *Z*-contrast. Ordered area is narrow and limited for some small nanoparticles.

dering can proceed in all three directions for the $L1_0$ phase. For a nanoparticle shown in Fig. 4(d), the {110} fringes of the $L1_0$ structure are observed in several parts of the nanoparticle.

To further confirm the atomic structures detected by HAADF-STEM, we examined the contrast of the STEM images and compared with the simple models based on projected potential. The results are shown in Fig. 5. In the $L1_0$ structure, each (001) atomic plane is composed of only Fe or Pd if we assume the degree of order as unity. When this structure is projected along the [001] direction, periodic arrangement of Fe and Pd atoms are observed. Figures 5(a) and 5(b) show the structure of the ordered FePd along the [001] and [110] directions, respectively, in the form of the square of the projected potential. The square is used to mimic the Z^2 dependence expected for the HAADF-STEM contrast based on the atomic scattering model. The similarity between the observed STEM image contrast and the projected potential is clearly observed here. The same agreement is also obtained for the ordered $FePd_3$ with $L1_2$ structure as shown in Figs. 5(c) and 5(d). In Fig. 5(d), the nanoparticle is rotated about 1° off the zone axis around the *a*-axis. This results in a streaked contrast from the Pd plane, which is observed in Fig. 4(a). The results here demonstrate that intensity modulation due to chemical order in a small $L1_0$-FePd nanoparticle is clearly imaged by C_s-corrected HAADF-STEM observation. Figure 6 simulates the core-shell effect on the

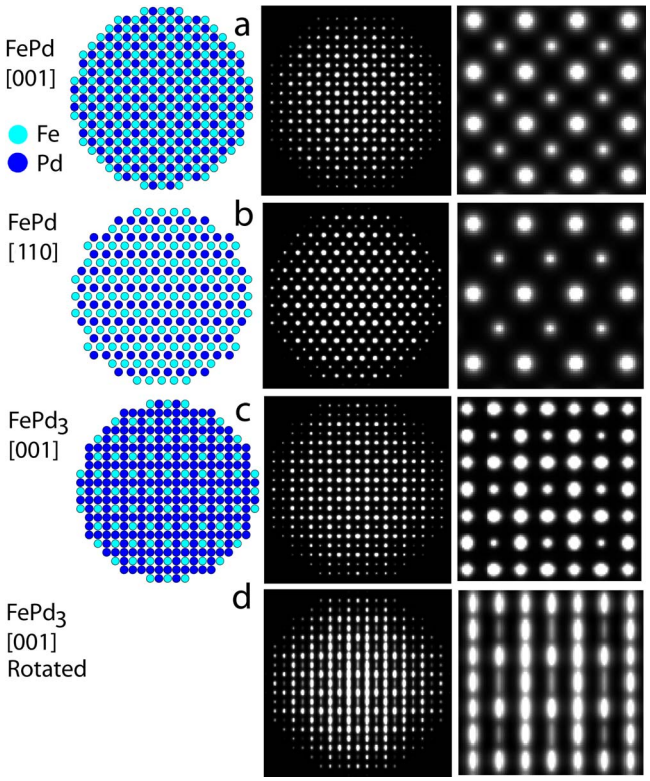

FIG. 5. (Color online) Structure models and the square of the simulated projected potential for the $L1_0$ ordered FePd and the $L1_2$ ordered $FePd_3$ nanoparticles. (a) along [001]$L1_0$, (b) [110]$L1_0$, (c) [001]$L1_2$, (d) rotated about 1° off the [001]$L1_2$ zone axis around the *a*-axis. Images on the right highlight the contrast in the middle of the model nanoparticles.

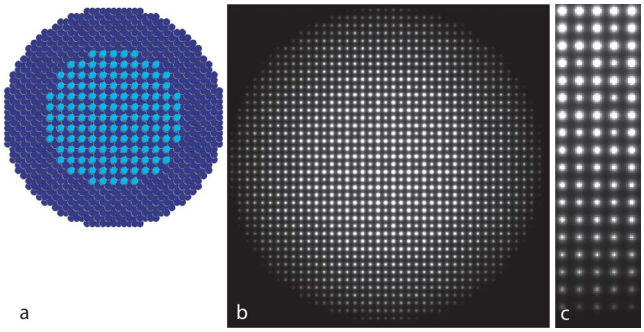

FIG. 6. (Color online) (a) A structure model of an 8 nm diameter core-shell nanoparticle with a 5 nm diameter ordered $FePd_3$ core and a solid solution of FePd for the shell (dark atoms). The square of the simulated projected potential for the nanoparticle is shown in (b). (c) A section of (b) from the center to the edge of the nanoparticle.

image contrast for an 8 nm diameter nanoparticle with a 5 nm diameter core made of ordered $FePd_3$ and an Fe rich shell made of Fe–Pd solid solution. This contrast difference between the Fe and Pd columns from the ordered core is clearly visible at the center of the nanoparticle, which becomes smaller near the edge of the core. The contrast difference depends on the relative thickness of the core and the shell in this case. For HAADF-STEM, there is also an additional limit to the overall thickness above which the contrast dependence on Z breaks down. Our experimental results suggest that nanoparticles studied here are small enough and the ratio of ordered and disordered phases is high enough to see the Z-contrast differences.

Thus, microscopy results show the presence of both the $L1_0$ and $L1_2$ structures in the nanoparticles. The $L1_2$-type ordered phase of the Fe–Pd alloy ($FePd_3$) occurs in a wide composition range between 62 and 86at. % Pd. The presence of $L1_2$ structure is thus an indication of Pd-rich phase. The $L1_2$-phase formation was recently reported for chemically synthesized FePt nanoparticles.[24] There are two possible reasons for the Pd-rich phase. One is chemical composition variation among different nanoparticles and the other is limited diffusion. Both are related to the sequential deposition process used to form these nanoparticles.

The Pd islands were formed first and each of Pd islands acts as the nucleation and growth center for the Fe atoms. According to the previous study using the same sample preparation technique,[12] the alloy composition distribution of the nanoparticles followed a Gaussian function and the standard deviation was about 4at. % (Ref. 12) based on the elemental analyses by EDX using an electron nanoprobe. Also the alloy composition showed no obvious particle size dependent distribution.[12] According to this alloy composition distribution, we estimate the minimum and maximum compositions of 50at. % Pd and 62at. % Pd, respectively, for the average composition of 58at. % Pd. The $L1_0$ phase is formed at the composition range between 50 and 60at. % Pd. The population of FePd nanoparticles exceeding 60at. % Pd is as small as 5% in the histogram. These results indicate that a rather small alloy composition distribution may still cause a difference in atomic ordering and possibly lead to a partial formation of $L1_2$ phase as observed in the present study.

The Z-contrast images show two interesting features. First, inside each nanoparticle, the ordered region is associated with high, bright, contrast, while the disordered region, often at the periphery of the nanoparticle, shows dark contrast. While the reduced thickness of the nanoparticles near the particle edge may contribute to such contrast changes, it should be noted that the observed contrast change can also indicate the existence of a Pd-rich region at the central part of nanoparticles, which will be consistent with the observation of $L1_2$ phase in the middle of some nanoparticles. In other words, these experimental results suggest a limited diffusion that leads to a Pd-rich core for the $L1_2$ phase formation. The existence of Pd-rich region at the central part of nanoparticles is highly plausible because of the sequential deposition of Pd and Fe, where the formation of an alloy requires exchange of Pd and Fe with Pd diffusing out from the center of the nanoparticle and Fe diffusing into the center. The Pd-rich core indicates an incomplete exchange process.

The second feature of the Z-contrast images is the size of the ordered region. The ordered regions in the nanoparticle shown in Fig. 4(d) extends over an area as large as 6 nm, while the 4-nm-sized nanoparticle in Fig. 4(a) or the 6-nm-sized nanoparticle in Fig. 4(b) are less ordered. Further, the ordered region of the larger 8-nm-sized [Fig. 4(c)] nanoparticle is also small and limited to some local areas. The annealing carried out here was intentionally performed at a lower temperature of 835 K for a short period of 10 min, compared to the previous reports (973 K-24 h or 1073 K-4 h,[11] 873 K-1 h or 10 h[10,12]), in an attempt to observe the intermediate stages of chemical ordering. It is interesting that partially ordered region was also observed in smaller sized FePd nanoparticles [Figs. 4(a) and 4(b)].

The results here show that HAADF-STEM can be used to detect inhomogeneous alloying because of the large difference in atomic numbers (Z) for Pd and Fe at $Z_{Pd}=46$ and $Z_{Fe}=26$, respectively. The contrast ratio of Fe from Pd in the HAADF-STEM image is 3.1 if we expect a Z^2 dependence of image intensity. Existence of central bright contrast region surrounded by dark contrast area indicates alloying of Fe into Pd nanoparticles, followed by atomic ordering at the alloyed region. This is expected at the initial stage of atomic ordering by annealing. Prolonged annealing is expected to promote further exchange of Fe and Pd leading to more homogeneous nanoparticles.

IV. CONCLUSION

We have studied epitaxial island formation, alloying, and chemical ordering of FePd nanoparticles by *in situ* RHEED, HREM, and C_s-corrected HAADF-STEM. Epitaxial Fe/Pd nanoparticles were formed by successive deposition of Pd and Fe onto single crystal NaCl(001) substrate kept at 560–570 K. The epitaxial island growth and subsequent alloying of Fe into Pd were clearly detected by RHEED, which showed initial appearance of spotlike reflections of fcc-Pd and bcc-Fe, followed by disappearance of the Fe reflections upon annealing. The orientation relationship between fcc-Pd and NaCl, and bcc-Fe and fcc-Pd deduced from RHEED

patterns are $[100]_{Pd}\|[100]_{NaCl}$, $(001)_{Pd}\|(001)_{NaCl}$, and $[\bar{1}10]_{bcc\text{-}Fe}\|[100]_{Pd}$, $(001)_{bcc\text{-}Fe}\|(001)_{Pd}$, respectively. The alloying proceeded rapidly in a narrow temperature range between 710 and 730 K as detected by the disappearance of the Fe reflections in RHEED patterns. After annealing at 775 K for a short period of time, a $L1_0$-type ordered phase was detected by SAED and HREM in FePd nanoparticles. However, the ordered region was limited to a small area, and the intensity of the superlattice reflections was weak in the SAED pattern. Further examination using C_s-corrected HAADF-STEM revealed local chemical order in FePd nanoparticle with both the $L1_0$- and $L1_2$-type structures. We interpret the presence of the $L1_2$-type phase based on kinetically limited atomic ordering, which proceeds by exchange of Pd and Fe between the heavy Pd-rich core and light Fe-rich periphery. Alloy composition distribution can also lead to the formation of $L1_2$ phase. The results here demonstrate the complexity of chemical ordering in alloy nanoparticles and the power of aberration corrected HAADF-STEM for studying nanoscale chemical ordering.

ACKNOWLEDGMENTS

This work was supported by NSF Grant No. DMR 0449790. The electron microscopy and Rutherford backscattering spectroscopy were carried out in the Center for Microanalysis of Materials, University of Illinois, which is partially supported by the U.S. Department of Energy under grant No. DEFG02-91-ER45439. One of the authors (K.S.) wishes to thank W. J. Huang, S. Sivaramakrishnan, and W. Sweich for their help using the RHEED chamber.

[1]D. Weller and M. F. Doerner, Annu. Rev. Mater. Sci. **30**, 611 (2000).
[2]H. Shima, K. Oikawa, A. Fujita, K. Fukamichi, K. Ishida, and A. Sakuma, Phys. Rev. B **70**, 224408 (2004).
[3]S. Ostanin, S. S. A. Razee, J. B. Staunton, B. Ginatempo, and E. Bruno, J. Appl. Phys. **93**, 453 (2003).
[4]H. Naganuma, K. Sato, and Y. Hirotsu, J. Magn. Magn. Mater. **310**, 2356 (2007).
[5]S. Sun, C. B. Murray, D. Weller, L. Folks, and A. Moser, Science **287**, 1989 (2000).
[6]M. Tanase, N. T. Nuhfer, D. E. Laughlin, T. J. Klemmer, C. Liu, N. Shukla, X. Wu, and D. Weller, J. Magn. Magn. Mater. **266**, 215 (2003).
[7]S. Kang, Z. Jia, D. E. Nikles, and J. W. Harrell, J. Appl. Phys. **95**, 6744 (2004).
[8]B. Bian, K. Sato, Y. Hirotsu, and A. Makino, Appl. Phys. Lett. **75**, 3686 (1999).
[9]K. Sato, B. Bian, and Y. Hirotsu, Jpn. J. Appl. Phys., Part 2 **39**, L1121 (2000).
[10]K. Sato and Y. Hirotsu, J. Appl. Phys. **93**, 6291 (2003).
[11]H. Pan, S. Fukami, J. Yamasaki, and N. Tanaka, Mater. Trans. **44**, 2048 (2003).
[12]K. Sato, Y. Hirotsu, H. Mori, Z. Wang, and T. Hirayama, J. Appl. Phys. **98**, 024308 (2005).
[13]J. L. Hutchison, J. M. Titchmarsh, D. J. H. Cockayne, R. C. Doole, C. J. D. Hetherington, A. I. Kirkland, and H. Sawada, Ultramicroscopy **103**, 7 (2005).
[14]K. Fukaya, S. Ino, and S. Ogawa, Trans. Jpn. Inst. Met. **19**, 445 (1978).
[15]M. Gillet and A. Renou, Surf. Sci. **90**, 91 (1979).
[16]G. Rupprechter, K. Hayek, L. Rendón, and M. José-Yacamán, Thin Solid Films **260**, 148 (1995).
[17]F. Robinson and M. Gillet, Thin Solid Films **98**, 179 (1982).
[18]B. Q. Li and J. M. Zuo, Phys. Rev. B **72**, 085434 (2005).
[19]F. K. LeGoues, M. Liehr, M. Renier, and W. Krakow, Philos. Mag. B **57**, 179 (1988).
[20]C. S. Barrett and T. B. Massalski, *Structure of Metals*, 3rd ed. (McGraw-Hill, New York, 1966).
[21]K. Sato and Y. Hirotsu, Trans. Mater. Res. Soc. Jpn. **29**, 1647 (2004).
[22]B. Bian, D. E. Laughlin, K. Sato, and Y. Hirotsu, J. Appl. Phys. **87**, 6962 (2000).
[23]A. Kovács, K. Sato, and Y. Hirotsu, J. Appl. Phys. **101**, 033910 (2007).
[24]J. E. Wittig, J. Bentley, L. F. Allard, M. S. Wellons, and C. M. Lukehart, Microsc. Microanal. **14**, 348 (2008).